Tellus (2002), 54A, 205–219
Printed in UK. All rights reserved

TELLUS
ISSN 0280–6495

Atmospheric drag coefficients over sea ice — validation of a parameterisation concept

By THOMAS GARBRECHT, CHRISTOF LÜPKES*, JÖRG HARTMANN and MAREILE WOLFF, *Alfred Wegener Institute, Foundation for Polar and Marine Research, Postfach 120161, D-27515 Bremerhaven, Germany*

(Manuscript received 10 October 2000; in final form 29 October 2001)

ABSTRACT

The concept of drag partitioning to parameterise the surface roughness of sea ice is validated using topography data of regions with high sea ice concentrations. The parameterised drag is compared to measurements obtained by aircraft and ship. The form drag can well be expressed as a function of mean ridge heights and spacings averaged over flight legs of 12 km, if an improved approximation for the coefficient of resistance of a single ridge is used. We find a good agreement between the parameterised and observed drag coefficients. The highest sea ice roughness was encountered close to coastal regions and the lowest in the central Arctic.

1. Introduction

Regional variations in the sea ice roughness are often not adequately represented in parameterisations used in atmospheric models. A simple concept that accounts for the variation of the sea ice roughness due to ice ridges was introduced by Arya (1973; 1975). This concept distinguishes between the influence of small-scale roughness (skin drag) and larger distinct obstacles (form drag) on the total surface roughness. Both depend on the regional ice conditions, the latter more strongly, and it can be expressed as a function of regional averages of ridge heights and spacings. Thus, different ice conditions can be accounted for with only few surface information. Joffre (1983) used the concept of Arya to estimate drag coefficients over Baltic sea ice. He found a good qualitative agreement between observed and calculated drag coefficients, but considerable quantitative uncertainties. Mai et al. (1996) applied the concept to the marginal ice zone, where the form drag mainly results from floe edges.

It is the main goal of the present paper to validate the skin drag/form drag concept by use of observations over regions with high ice concentration where the form drag mainly results from pressure ridges rather than from floe edges. The analysis of Mai et al. (1996) was based on the knowledge of the actual probability density distributions of the ridge height and the spacing of floes. Mostly, however, this detailed information is not available from observations or sea ice models. In the present paper we show that the parameterisation scheme is well applicable for situations with only mean values of the ridge height available. The form drag parameterisation is based on a formulation of Garbrecht et al. (1999) for a case study of the flow around a single pressure ridge of 4.5 m height. It is extended to diabatic conditions and tested with data from ship and aircraft, which will be described in the following section. The form drag concept is explained in Section 3, and a validation of the parameterisation follows in Section 4.

* Corresponding author.
e-mail: cluepkes@awi-bremerhaven.de

2. Measurements of turbulence and ice topography

2.1. *ARTIST*

2.1.1. Turbulence measurements. During the Arctic Radiation and Turbulence Interaction Study (ARTIST) (Hartmann et al., 1999) a 150 km long return flight, 30 m above sea level, was performed by the aircraft Polar 2 on 16 March 1998. It was equipped with a turbulence probe and a laser altimeter. The flight was first inbound from the ice edge (at position A in Fig. 1) towards the coast of Svalbard (position B) and returned outbound. The large-scale meteorological conditions during the flight are characterized by an on-ice flow situation with slight cooling over the ice due to a 3 K difference between the surface temperature of sea ice and the air temperature. During the measurements of approximately 1.5 h duration no significant temporal change of the flow direction and the wind velocity was observed.

The measurements of each flight leg (inbound and outbound) are subdivided into 11 sections of approximately 12 km length (corresponding to 3 min measuring time for the aircraft). Figure 2 shows the observed absolute value of wind, the heat fluxes, and the stability parameter $10/L$ as a function of the distance to position A. The wind speed decreases slightly from A towards B. Its leg-averaged value amounts to 8.7 m s^{-1}. The stability changes from slightly stable near the open ocean (A) to near-neutral towards the coastline of Svalbard (B). The absolute values of the downward heat fluxes increase from 10 W m^{-2} at position A to 20 W m^{-2} at position B, while the stability is decreasing. This indicates that the atmospheric turbulence during the flight is predominantly influenced by the underlying ice surface. Without a change in surface roughness a decreasing stability would result in decreasing fluxes.

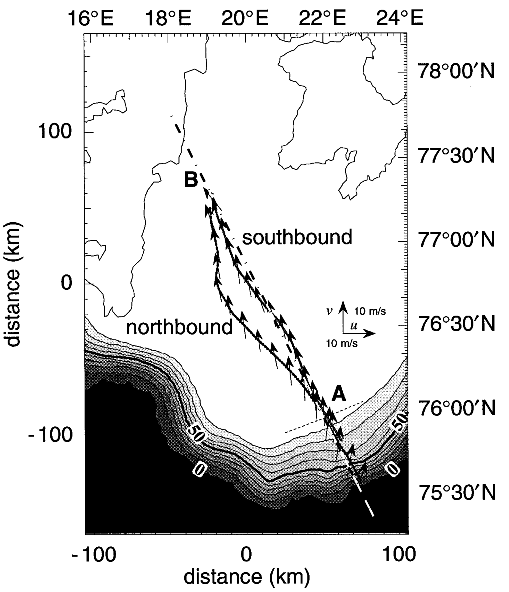

Fig. 1. The flight path southeast of Svalbard flown by research aircraft Polar 2, on 16 March 1998 during ARTIST. Arrows represent the wind vector during the flight mission. The grey shading in the lower part of the map indicates the ice concentration (given in percent) derived from SSM/I data by a method of Heygster and Kaleschke (2000).

2.1.2. Ice topography. The ice surface topography was measured by a laser altimeter with a horizontal resolution of 10 cm and a vertical accuracy of 2 cm. The determination of the topography from the laser signal requires the exact knowledge of the aircraft height. The latter is obtained by the inertial navigation system (INS) with sufficient accuracy for horizontal scales up to 1 km. Thus, the measurements resolve scales from 0.1 to 1000 m. In order to detect ridges from the laser signal a minimum ridge height of 20 cm is prescribed. The so-called Rayleigh criterion (Dierking, 1995) is used to count strongly fissured ridges as a single ridge. This criterion requires a maximum of the topography curve to twice exceed both neighbouring minima.

The visual observation from the aircraft indicated that the ice conditions changed from a very smooth surface near position A to a rough surface at position B. This is confirmed by the results of the topography measurements (Fig. 3). They show that the ensemble ridge heights H_e increase by a factor of about 1.7 from position A to position B, whereas the spacing of ridges Δx_e is decreasing. This results in increasing aspect ratios $A_e = H_e/\Delta x_e$ and increasing drag coefficients from A to B (Fig. 3). We discuss this finding in more detail in the following sections.

All topography data follow very well the probability density functions (PDF) for the ridge height

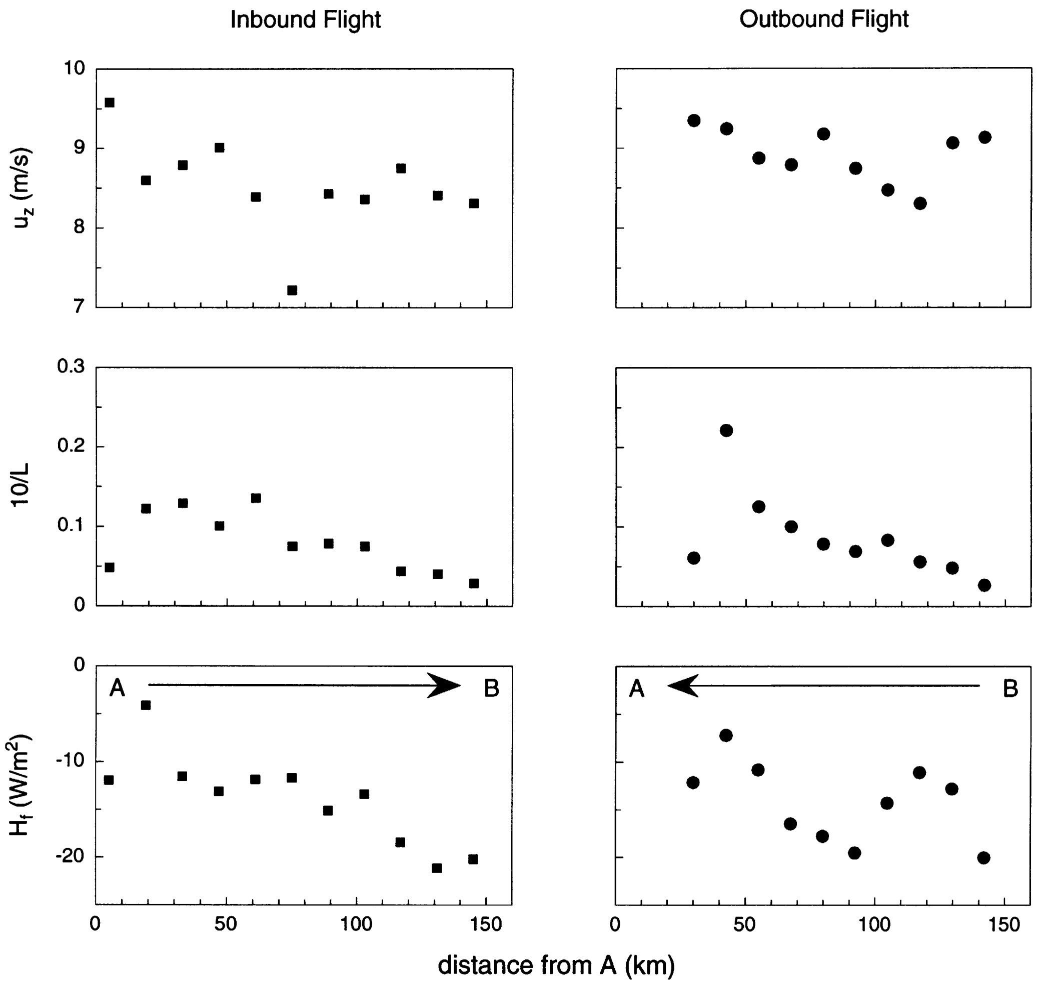

Fig. 2. Wind speed u_z, atmospheric stability $10/L$ and the sensible heat flux H_f as measured during the campaign ARTIST.

in the form proposed by Wadhams (1980)

$$p(H_R)\,dH_R = a \exp(-aH_R)\,dH_R \tag{1}$$

and for the ridge spacing as used by Hibler et al. (1972)

$$p(\Delta x)\,d\Delta x = b \exp(-b\Delta x)\,d\Delta x. \tag{2}$$

$p(H_R)$ and $p(\Delta x)$ are the number densities of ridges with height H_R in the infinitesimal interval $[H_R, H_R + dH_R]$ and with spacing Δx in the interval $[\Delta x, \Delta x + d\Delta x]$, respectively. The parameter a can be calculated as a function of the mean ridge height with a prescribed threshold value for the minimum ridge height, and the parameter b as a function of the mean spacing, respectively. As an example we show in Fig. 4 the PDF for ridge heights of a typical 12 km section of smooth ice (left) and of rough ice (right). The figure contains the PDF calculated with eq. (1) (solid lines) as well as the distributions (histograms) observed during ARTIST. The same quality of agreement between the observed and calculated PDF with eq. (1) occurs for the other flight sections as well, and similar results are obtained for the PDF of the ridge distance, eq. (2).

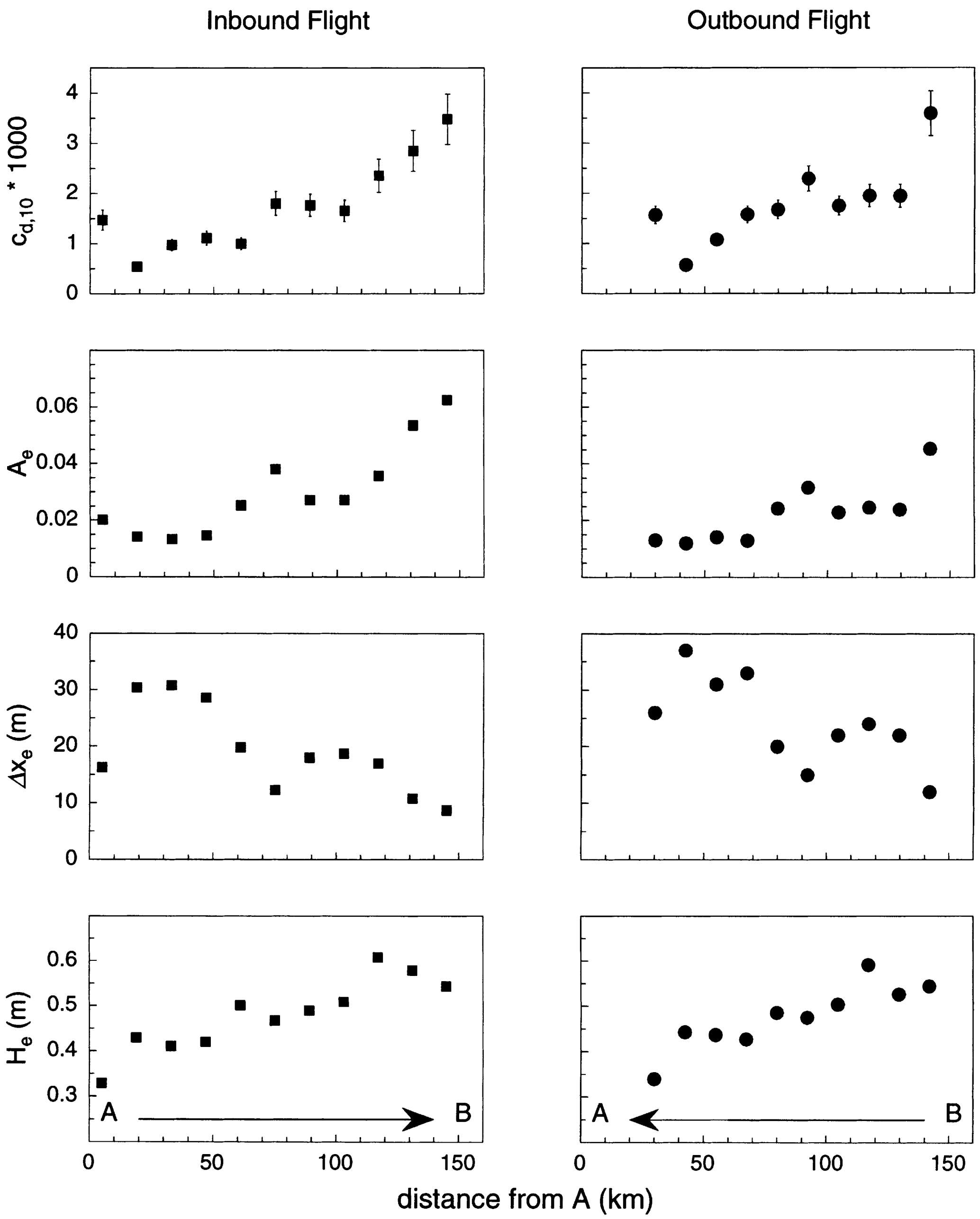

Fig. 3. Drag coefficients $c_{d,10}$, aspect ratio A_e, ridge spacing Δx_e, and mean ridge height H_e as measured during the campaign ARTIST.

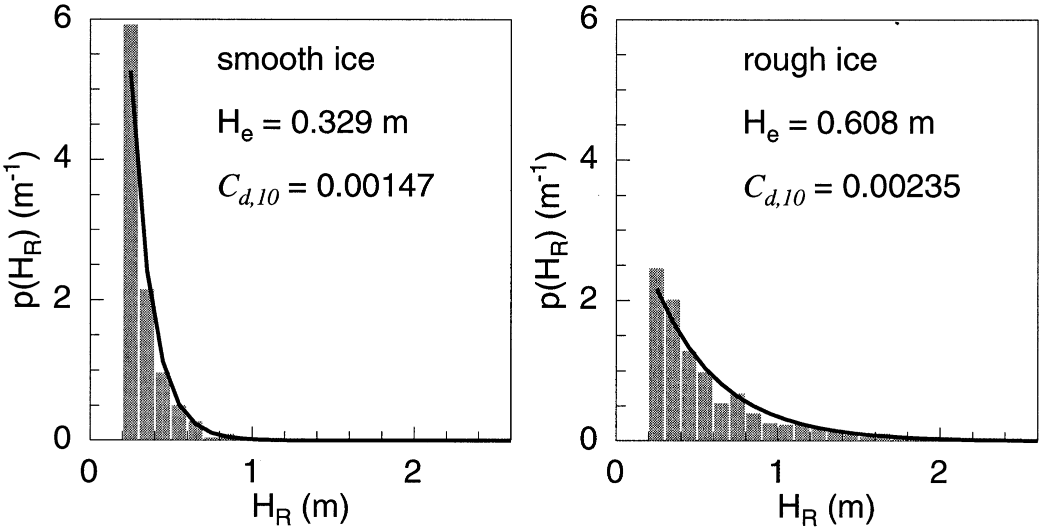

Fig. 4. Histograms of ridge height distributions for smooth ice (left) and rough ice (right). The solid lines were calculated by eq. (1) and the grey bars represent ARTIST measurements. Each histogram represents a 12 km section of the flight.

2.2. ACSYS

2.2.1. Turbulence measurements. Cruise ARCTIC '96 (Fig. 5) of research vessel *Polarstern* (Augstein et al., 1997) was carried out in the framework of the Arctic Climate System Study (ACSYS). Turbulence measurements were performed by a turbulence measuring system (TMS) (Garbrecht et al., 1999) in the central Arctic during summer at positions marked with triangles in Fig. 5. The TMS consists of sonic anemometers installed on a vertical mast at the bow crane of RV *Polarstern* at 8 and 13 m height.

The meteorological conditions differ from the ARTIST experiment mainly by the absolute value of the mean wind, which amounts to only 1.8–3.7 m s^{-1} interpolated to 10 m height and averaged over periods of 30 min. This is much lower than the 8.7 m s^{-1} during the ARTIST case study, but it represents the typical situation during the total cruise of 3 months duration. Except for 17 August, the stratification was close to neutral ($|10/L| \approx 0$, see Table 1).

2.2.2. Ice topography estimates. Figure 6 shows a measuring site during ARCTIC '96 (27 July, view from *Polarstern*). The image illustrates that an

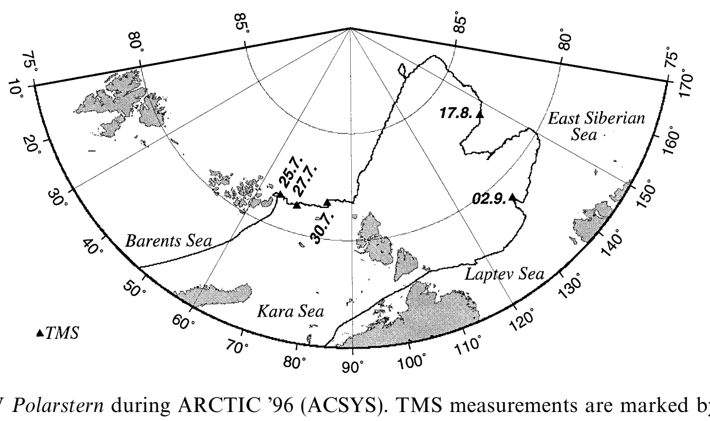

Fig. 5. Track of RV *Polarstern* during ARCTIC '96 (ACSYS). TMS measurements are marked by triangles.

Table 1. *Mean values of ridge height, ridge spacing, $10/L$ and $\overline{u_{10}}$ for the ACSYS case studies*

Date	H_e (m)	Δx_e (m)	$10/L$	$\overline{u_{10}}$ (m s^{-1})
07/25	1.50	150.0	−0.048	3.7
07/27	1.50	50.0	0.016	1.9
07/30	1.00	50.0	0.060	3.3
08/17	1.00	100.0	−0.448	1.8
09/02	1.50	250.0	0.072	3.1

assumption of more or less homogeneous ridges as in the form drag concept explained in Section 3 represents a strong idealisation. The ridges visible on the image are strongly fissured and irregular along the ridge axis.

During ARCTIC '96, mean ridge heights and spacings were determined from visual observations compiled by Lensu et al. (1996). Ridges, located in close vicinity of RV *Polarstern*, were counted and measured. The estimated mean heights have been separated into height classes of 0.5 m width. Errors of this determination cannot be specified, but they occur probably from an insufficient number of ridges in the vicinity of the ship. Also the width of height classes is relatively large, which may lead to errors in the form drag determination. Thus, the calculation of form drag based on the ship measurements has a larger uncertainty than that based on the aircraft measurements.

3. Surface drag coefficient

3.1. Drag partitioning

According to Arya (1975), the total vertical flux of momentum can be expressed as the sum of a skin effect $\tau_{0,s}$, representing the microscale roughness of the surface, and of a form effect $\tau_{0,f}$, which results from the influence of single obstacles. In case of polar regions, these obstacles are present in form of pressure ice ridges and the edges of ice floes. Considering the drag partitioning theory, the total drag coefficient c_{d,z_r} at reference height z_r results as the sum of the coefficients for skin drag (index s) and form drag (index f):

$$c_{d,z_r} = c_{d,z_r,s} + c_{d,z_r,f}. \tag{3}$$

To apply this concept to model simulations, the knowledge of both the skin and the form drag coefficient is required. Both depend on the underlying surface and on the density stratification of the atmosphere.

3.2. Skin drag

The skin drag coefficient is obtained by use of the stability corrected logarithmic wind profile

$$u_z = \frac{u_*}{\kappa}\left[\ln\frac{z}{z_0} - \Psi_m\left(\frac{z}{L}\right)\right], \tag{4}$$

with the Dyer–Businger stability function $\Psi_m(z/L)$. L is the Monin–Obukhov length. With the defini-

Fig. 6. Measuring site of 27 July 1996 (ACSYS case) with the mast at the bow crane of RV *Polarstern*. The arrow represents the direction of the mean surface wind.

tion $c_{d,z_r,s} = u_*^2/u_{z_r}^2$ the skin drag coefficient at height z_r follows as

$$c_{d,z_r,s} = \left(\frac{\kappa}{\ln(z_r/z_0) - \Psi_m(z_r/L)}\right)^2, \tag{5}$$

if we assume that z_r is within the constant flux layer. This concept requires the knowledge of an adequate roughness length that represents the conditions over smooth ice. In the present study we apply $z_0 = 1.0 \times 10^{-5}$ m, which can be derived from aircraft measurements as shown in Section 4.4.

3.3. *Form drag*

The vertical flux of momentum induced by a single obstacle can be expressed by (Hanssen-Bauer and Gjessing, 1988):

$$\tau_{0,1} - \frac{\rho}{2} c_w \frac{1}{\Delta x} \int_{z_0}^{H_R} u_z^2 \, dz. \tag{6}$$

The parameter c_w is the coefficient of resistance of a single obstacle of height H_R, and Δx is the horizontal distance downstream of the ridge at which the mean vertical wind profile is assumed to be restored to its undisturbed stage. With $\tau_{0,f} = \rho c_{d,z_r,f} u_{z_r}^2$ and by use of eq. (4), the form drag coefficient can be derived as

$$c_{d,z_r,f} = \frac{1}{2} \frac{c_w}{\Delta x} \left(\frac{1}{\ln(z_r/z_0) - \Psi_m(z_r/L)}\right)^2 \times \int_{z_0}^{H_R} \left[\ln \frac{z}{z_0} - \Psi_m\left(\frac{z}{L}\right)\right]^2 dz. \tag{7}$$

$c_{d,z_r,f}$ is the form drag coefficient for an area covered homogeneously by obstacles of the same height H_R, of the same mean ridge spacing Δx and of an orientation rectangular to the mean wind. Although ice-covered regions show variations of these parameters, we can generalise eq. (7) to an ensemble of ridges with ensemble mean values for the ridge height (H_e) and the ridge spacing (Δx_e). The use of probability density functions of the ridge height and the ridge spacing as in Mai et al. (1996) only leads to marginal improvements.

Ridges are typically orientated randomly (Mock et al., 1972). The form drag is therefore reduced by a geometric factor $2/\pi$. Since wind measurements are mostly carried out at 10 m height and the lowest grid level in atmospheric models is also often at $z = 10$ m, drag coefficients are commonly related to 10 m. Hence, we can write

$$c_{d,10,f} = \frac{c_w}{\pi \, \Delta x_e} \left(\frac{1}{\ln(10/z_0) - \Psi_m(10/L)}\right)^2 \times \int_{z_0}^{H_e} \left[\ln \frac{z}{z_0} - \Psi_m\left(\frac{z}{L}\right)\right]^2 dz. \tag{8}$$

This parameterisation is only valid with the assumption of a large ridge spacing, so that the flow can return to its undisturbed state before passing the next ridge. Wind tunnel studies of Arya and Shipman (1981) as well as measurements by Garbrecht et al. (1999) have shown that the mean wind profile and the turbulence state are totally restored at a distance of about 65 times the ridge height, which corresponds to an aspect ratio $H_e/\Delta x_e = 0.015$. In case of the measurements discussed in Section 2, the observed A_e is, however, larger than the critical value 0.015. For this reason we evaluated the influence of ridge sheltering by introducing a simple parameterisation of this effect in eq. (8) as suggested by Hanssen-Bauer and Gjessing (1988). That parameterisation describes the mean wind field in the wake of an obstacle by reducing the undisturbed wind profile by a height constant factor which depends on Δx_e. However, the parameterisation changed $c_{d,10,f}$ by less than 3% in our cases, so that we neglect it in eq. (8).

3.4. *Coefficient of resistance* c_w *for a single ridge*

For an application of eq. (8) c_w needs to be known. Data of Banke and Smith (1975) (BS75) and of Garbrecht et al. (1999) show that c_w is a function of the ridge height (Fig. 7). This might be caused by a height dependence of the flank steepness, documented in BS75 and by an increase of surface irregularities with increasing ridge height. Based on measurements at five ice ridges of different height BS75 have suggested a linear formulation for c_w as a function of the ridge height

$$c_w = a_H + b_H H_R \quad \text{with } a_H = 0.05, \, b_H = 0.14 \text{ m}^{-1}, \tag{9}$$

where c_w was calculated by use of the wind speed at 10 m height. However, as c_w is commonly based on the wind speed at obstacle height, the values obtained by BS75 need to be adjusted. This has been carried out with the assumption of a logarithmic wind profile below the measuring height to

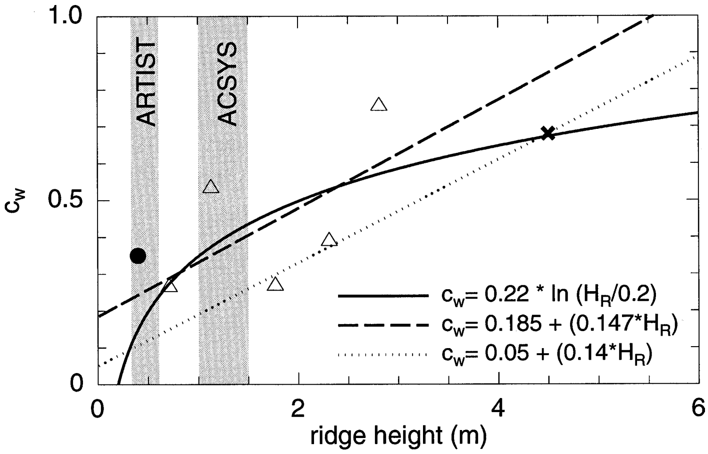

Fig. 7. Coefficient of resistance of a single ridge as a function of the ridge height calculated by different parameterisations (solid line, Garbrecht et al. (1999); dotted line, BS75; dashed line, BS75 with adjusted coefficients; triangles, observed by BS75 (adjusted values); cross, observed by Garbrecht et al. (1999); full circle, Garbrecht et al. (1999), reanalysed from observations. The shaded areas mark the range of observed mean ridge heights during ACSYS and ARTIST.

yield modified coefficients $\tilde{a}_H = 0.185$ and $\tilde{b}_H = 0.147\ \mathrm{m}^{-1}$.

Based on the modified data of BS75, on a further estimation of the c_w-value of an ice ridge with $H_R = 4.5$ m, and on an estimation of c_w for ice flow edges, Garbrecht et al. (1999) suggested the parameterisation

$$c_w = 0.22 \ln \frac{H_R}{0.2}, \quad \text{for } H_R > 0.2\ \mathrm{m}. \tag{10}$$

Results obtained with eqs. (9) and (10) are included in Fig. 7. The c_w-value of flow edges differs from that given in Garbrecht et al. (1999) because it is based on a reanalysis with more data of the campaign REFLEX (Kottmeier et al., 1994) included. This improved value (full circle in Fig. 7) would support the (modified) BS75 curve rather than the logarithmic curve, indicating that there is a lower limit for the flank steepness of ridges. However, more observations are necessary to confirm this. Hence, we present results obtained with both eqs. (9) and (10).

In the present study we consider the form drag mainly caused by ridges with mean heights between 0.3 and 0.6 m (campaign ARTIST) and between 1.0 and 1.5 m (campaign ACSYS). Both height ranges are marked in Fig. 7, and it is quite obvious that the modified BS75 c_w-values are higher than the Garbrecht et al. (1999) c_w-values in case of ARTIST and lower in case of ACSYS. The original BS75 values, however, are in both cases much lower than the other values.

4. Observed and calculated drag coefficients

4.1. Statistical error of flux measurements

The statistical uncertainties of the airborne measured drag coefficients are related to the statistical error of flux measurements, which depend on the length of the flight path, on the measurement height and on the temperature lapse rate. For neutral conditions the relative uncertainty α of the covariance $[(\overline{u'w'})^2 + (\overline{v'w'})^2]^{1/2} = u_*^2$ can be estimated from the length of the flight path l and the measurement height z by (Wyngaard, 1973):

$$\alpha = \left(\frac{20z}{l}\right)^{1/2}. \tag{11}$$

This estimation results in errors of 20% for the aircraft data. For the mast measurements eq. (11) can be used when l is replaced by $|u|t$, the mean wind speed multiplied with averaging time. The resulting errors also amount to about 20%.

4.2. *Influence of fetch on the drag coefficients*

The aircraft observations are adequate to check the form drag concept only if the drag coefficients are close to equilibrium values. Hence, we used the two-dimensional (2D) nonhydrostatic mesoscale model METRAS (Schlünzen, 1990; Lüpkes and Schlünzen, 1996) to evaluate the fetch dependence of drag coefficients. The model is applied to the atmospheric boundary layer flow over sea ice with a prescribed step change in surface roughness. It is run with a horizontal grid length of 400 m and a vertical grid length of 4 m up to 50 m height (while increasing by a factor of 1.2 at each level above 50 m). A Mellor and Yamada (1974) type turbulence closure is used above the surface layer. Hence, eddy diffusivities are calculated as a function of the turbulent kinetic energy and of a mixing length. Surface fluxes follow from the Monin–Obukhov theory.

The model is initialised with profiles of wind and temperature being typical for the meteorological conditions during the ARTIST measurements (near-neutral stratification below 150 m with a strong inversion above that level). At the surface the temperature is prescribed constant to 270 K. The surface roughness is kept constant during the first 10 km of the 60 km total domain with $z_0 = 10^{-3}$ m, and a step change in roughness occurs further downstream ($z_0 = 10^{-2}$ m).

Figure 8 (top) shows modelled drag coefficients

$$c_{\mathrm{d},z} = \left. \frac{[(\overline{u'w'})^2 + (\overline{v'w'})^2]^{1/2}}{u^2 + v^2} \right|_z , \qquad (12)$$

at $z = 10$ m, $z = 22$ m, and $z = 30$ m (typical level of aircraft measurements) as a function of the distance x to the position of the roughness change. The lower graph represents the drag coefficients normalised by their equilibrium values at $x = -60$ km. Obviously, within only the first 2 km downstream of the roughness change there is a significant difference between the modelled drag coefficients and their equilibrium values, which are underestimated if the surface changes from smooth to rough. In case of leg lengths of 12 km the resulting error is in the order of 5%.

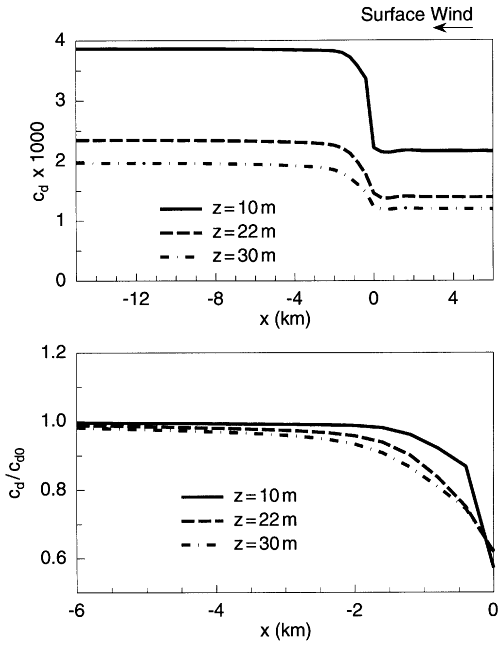

Fig. 8. Drag coefficients c_d obtained by the model METRAS as a function of the distance x to a step change in roughness z_0 (top: non-normalised values; bottom: normalised by their equilibrium values c_{d0} at $x = -60$ km). z_0 changes from 10^{-3} m ($x > 0$) to 10^{-2} m ($x < 0$).

4.3. *Extrapolation of drag coefficients to 10 m height*

Equation (12) is used to calculate 'observed' drag coefficients at height z from the observed wind and the observed variances. As the aircraft observations were carried out at 30 ± 5 m height, the drag coefficients need to be extrapolated to 10 m. We use a method applied earlier by Hartmann et al. (1994) which is based on results of a one-dimensional (1D) version of the model METRAS.

The latter has been run with the same high vertical resolution as the 2D version described in Section 4.2 and with the same typical initial temperature profile and geostrophic wind. Regarding the vertical profiles of drag coefficients obtained with these model runs the following ad hoc parameterisation results:

$$c_{\mathrm{d},10} = c_{\mathrm{d},z} \left(\beta + \frac{1-\beta}{10} z \right). \qquad (13)$$

Herein β is a constant which depends on the near-surface stratification. (Stable stratification was obtained by prescribing slight surface cooling after the wind profiles for neutral stratification became stationary.) Figure 9 shows model results for $c_{d,z}$ as a function of height as well as results of eq. (13) for neutral conditions. In all three cases the same value 0.692 for β was used, and the values for $c_{d,10}$ were prescribed in eq. (13) from the model result. Obviously the correction formula works sufficiently well. The same quality of agreement occurs for stable conditions.

4.4. *Stability effect on drag coefficients*

The drag coefficients $c_{d,10}$ obtained from the ARTIST observations are presented in Fig. 10 as a function of the aspect ratio A_e (top) and of the stability parameter z/L (bottom). From this figure it might be concluded that both aspect ratio and stability have a strong influence on $c_{d,10}$. However, a more detailed analysis reveals that during ARTIST the stability is correlated with A_e. For example, close to the ice edge the values of $10/L$ are the largest and values of A_e the smallest. For the typical range of stability and roughness during ARTIST and ACSYS ($|z/L| < 0.25$) the value of A_e has a much larger effect on the drag coefficients than the stability. This can be concluded from Fig. 11, which contains drag coefficients resulting from eqs. (5) and (8). Moreover, Fig. 11 shows that in case of rough sea ice with a large aspect ratio the form drag can exceed the skin drag significantly.

Figure 10 (top) contains a linear regression through all data points measured at near-neutral stratification ($|z/L| < 0.05$). Extrapolating the linear regression to $A_e = 0$ yields $c_{d,10} = 0.895 \times 10^{-3}$, which can be interpreted as neutral skin drag coefficient of very smooth ice. The roughness length thus follows from eq. (5) to be close to $z_0 = 1.0 \times 10^{-5}$ m. This value is applied in the following sections to calculate the total drag coefficients. It seems to be smaller than values mentioned by several other authors, but on the other hand it differs not too much from the value 1.6×10^{-5} m measured by Guest and Davidson (1991) over very flat ice.

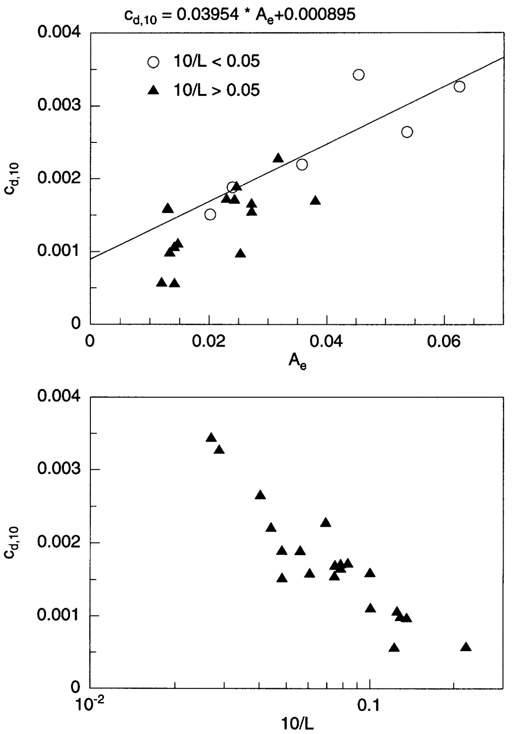

Fig. 10. Drag coefficients $c_{d,10}$ as a function of the aspect ratio $A_e = H_e/\Delta x_e$ (top) and of the stability parameter $10/L$ (bottom) for ARTIST. The upper graph contains a linear regression to all values obtained under near-neutral stratification ($10/L > 0.05$).

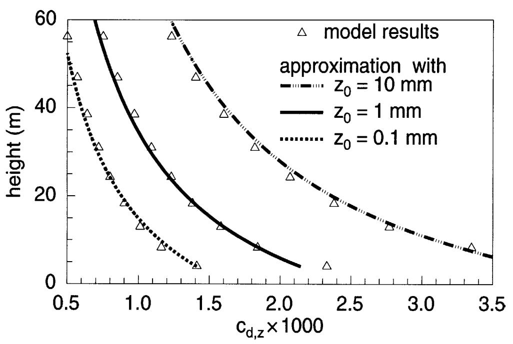

Fig. 9. Neutral drag coefficients $c_{d,z}$ as a function of height calculated with METRAS and with eq. (13), wherein $c_{d,10}$ is prescribed from the model result. The same value 0.692 is used for β in all three cases which differ by the prescribed roughness length.

4.5. *Comparison of airborne measured and parameterised drag coefficients*

With the information about the surface topography obtained by airborne and ground-based measurements, the total drag coefficient is calculated by eq. (3) with eq. (5) for the skin drag and

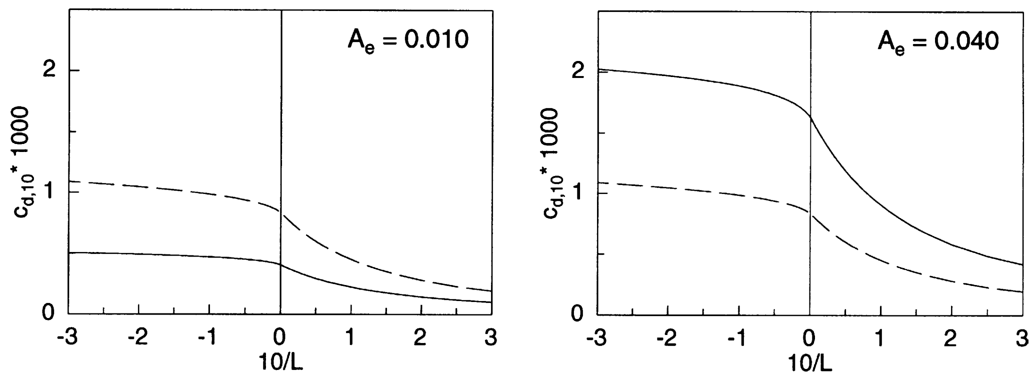

Fig. 11. Coefficients of skin drag (dashed line) and form drag (solid line) calculated with eqs. (3) and (8) as a function of $10/L$ for two different aspect ratios. In both cases the ridge height amounts to 0.6 m.

with eq. (8) for the form drag. For a quantitative comparison the parameterised $c_{d,10}$ is plotted in Fig. 12 versus the measurements. The figure contains information about the explained variance σ_f, which we define as

$$\sigma_f^2 = 1 - \frac{\overline{(y_i - \tilde{y}_i)^2}}{\overline{(y_i - \bar{y}_i)^2}}. \tag{14}$$

In eq. (14) y_i represent the measured drag coefficients in the ith flight section and $\tilde{y}_i$ are the parameterised ones. Thus, eq. (14) describes the amount of variance that is explained by the model.

The model values in Fig. 12 are based on the c_w parameterisations given by eq. (9) (with original and modified constants a_H, b_H) and by eq. (10). The solid line represents unity while the linear regression is presented by a dashed line. The results obtained with the original BS75 parameterisation for c_w strongly underestimate the measured values of $c_{d,10}$, while the results of both other parameterisations agree very well with the observations (with $\sigma_f^2 \sim 0.8$). $c_{d,10}$ calculated with c_w from eq. (9) (with reformulated constants) differs only slightly from $c_{d,10}$ calculated with c_w from eq. (10). This is due to the fact that both c_w parameterisations differ only slightly for the encountered range of H_R (Fig. 7).

The open symbols in Fig. 12 represent measurements where $A_e > 0.015$. Obviously, the drag coefficients at high A_e are not overestimated by the parameterisation, which confirms the finding, already discussed in Section 3.3, that sheltering effects do not reduce the form drag coefficient remarkably, at least for ice conditions as observed during ARTIST.

4.6. Comparison of shipborne measured and parameterised drag coefficients

A comparison of measured and modelled drag coefficients for the shipborne measurements is shown in Fig. 13, where the model values are based on the c_w-parameterisations given by eqs. (9) (original and modified) and (10). Observations marked with the same symbol type have all been carried out at the same geographical position. Hence, the variability of the observed drag coefficients for a fixed position is a result of the statistical error, of changing wind directions, and of different stabilities during the observation period. The variability of the calculated drag coefficients for a fixed position represents the influence of stability only (note, that only the average value of $10/L$ is given in Table 1).

Again there is a systematic underestimation of $c_{d,10}$ when eq. (9) is used with the original coefficients of BS75 to parameterise the coefficient of resistance. In both other cases, the parameterised and observed drag coefficients agree very well, with one exception (30.07.1996, marked with triangle). At that position a large ridge was observed close to the mast. Its distance to the mast was significantly smaller than the statistical average of ridge spacings in the environment.

The largest $c_{d,10}$ values occur on 27 July (circles in Fig. 13) when the ship was at a position east of

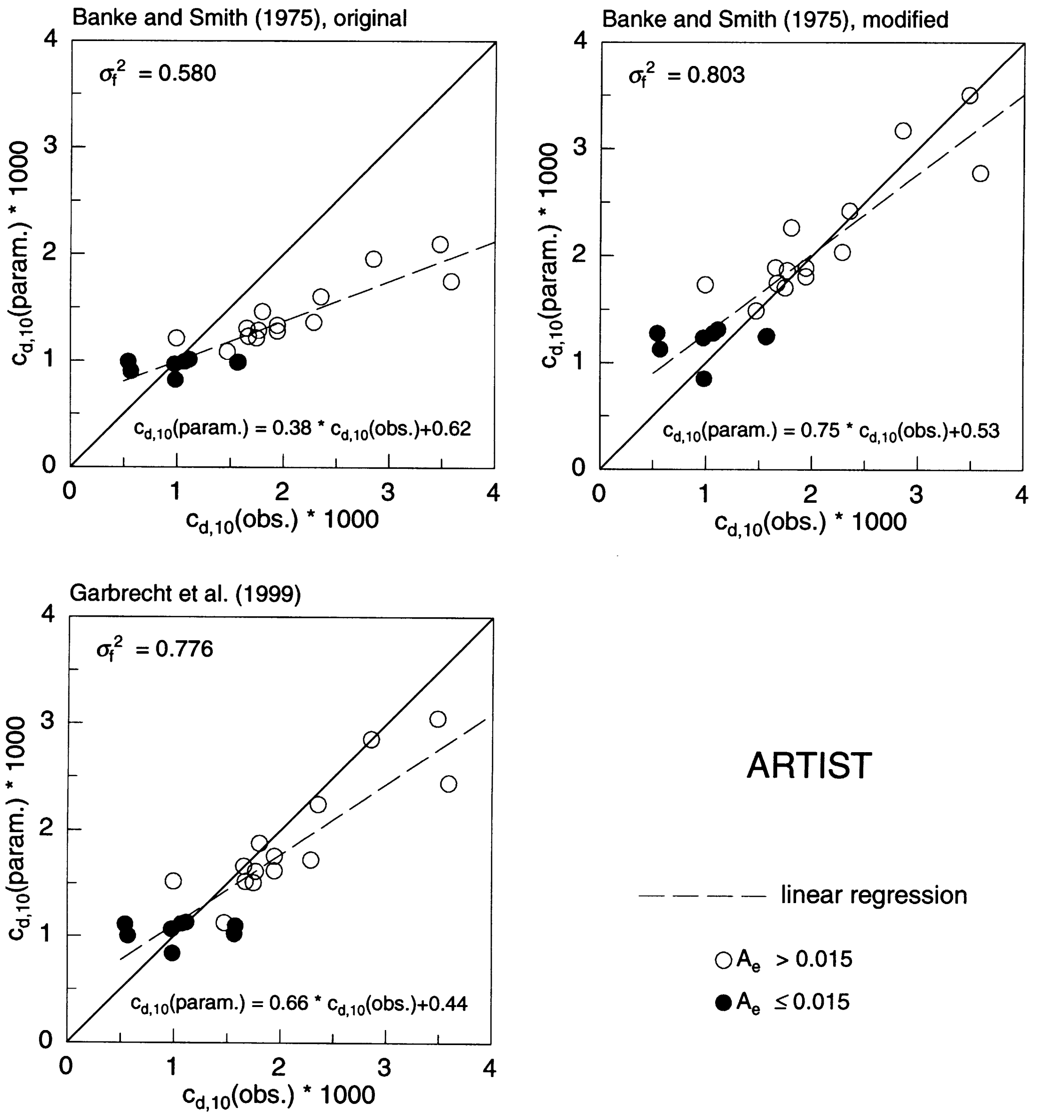

Fig. 12. Parameterised $c_{d,10}$ versus observed $c_{d,10}$ based on ARTIST measurements. The parameterised $c_{d,10}$ are calculated by three different formulae for c_w. Explained variances (upper left corner) and a linear regression (dashed lines) are given.

Franz-Josef-Land (Fig. 5). These values are well reproduced by the parameterisation.

5. Conclusions

Airborne and ship-based data from two different campaigns carried out in different regions of the Arctic have been analysed to derive drag coefficients from ice surface topography measurements. The highest values of the drag coefficients ($c_{d,10} > 2.5 \times 10^{-3}$) were encountered in coastal regions. In other regions they range from 1.2×10^{-3} to about 2.0×10^{-3}. This indicates that mainly in coastal regions the effect of form drag plays an important role due

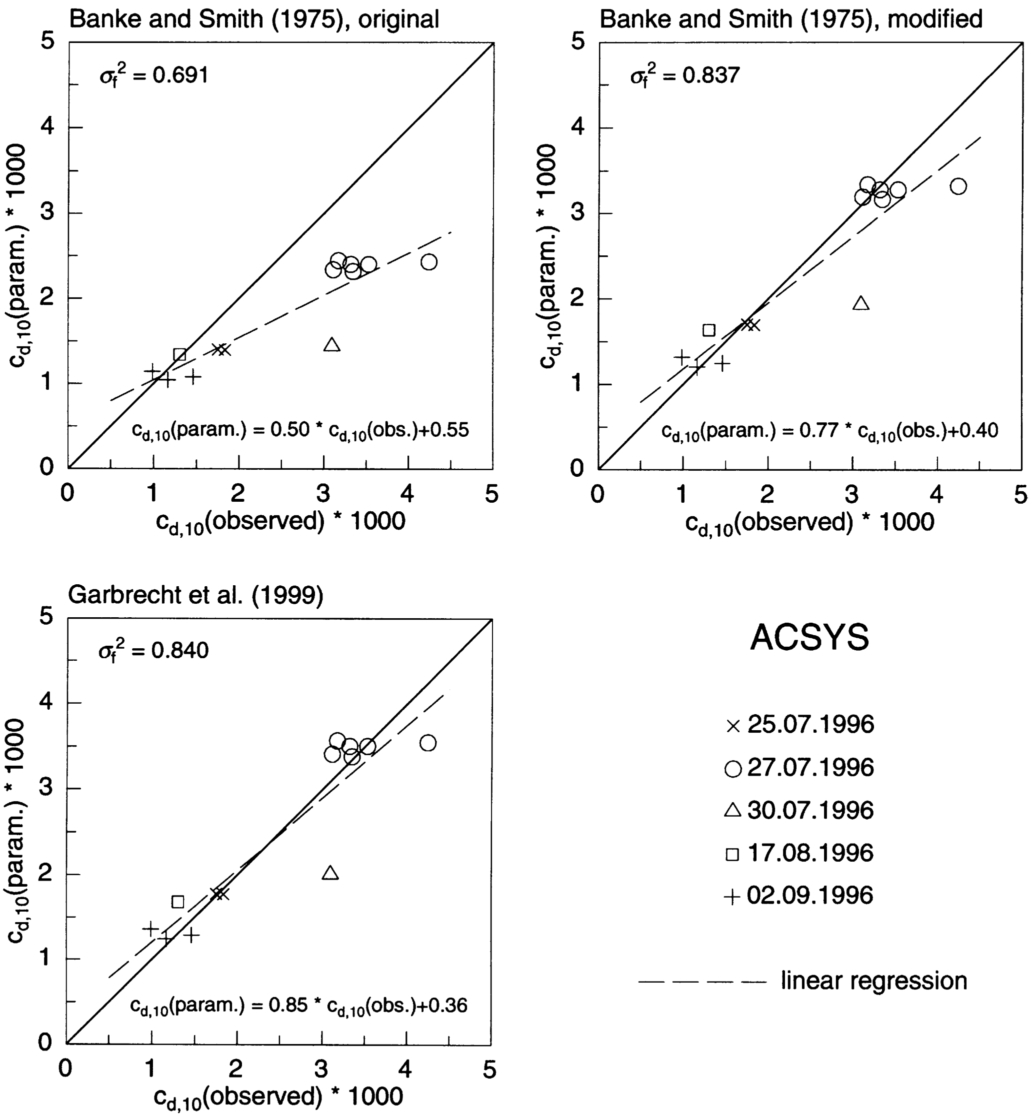

Fig. 13. Parameterised $c_{d,10}$ versus observed $c_{d,10}$ based on ship-borne measurements. The parameterised $c_{d,10}$ are calculated by three different formulae for c_w. Explained variances (upper left corner) and a linear regression (dashed lines) are given.

to higher ridges caused by accumulation of ice towards the land.

The measurements from two different sources have confirmed the validity of the concept of drag partitioning into skin drag and form drag. Despite the assumptions of equilibrium profiles and of height constant fluxes in the ridge influenced surface layer, the results of the parameterisation agree fairly well with the observed data. It appears that the form drag calculations are sufficiently accurate when only mean ridge heights and spacings are used in the parameterisation concept instead of probability density functions for both quantities. Our measurements confirm this for mean ridge heights 0.3 m < H_R < 1.5 m. This range probably holds for a very large part of the ice covered area in the Arctic. Further measurements are needed in areas of very small and very large mean ridge heights to extend the validation. Mean values of the ridge heights and spacings could be determined in future by sea ice models or from satellite observations as those used by Haas et al. (1999). They showed that the determination of the aspect ratio is possible from ERS SAR signatures. At present such detailed information is not available for the entire Arctic. However, based on our results we suggest to use in large-scale models a drag parameterisation that distinguishes between ice in coastal regions and on the open ocean. We propose to carry out further measurements in order to confirm this assumption.

6. Acknowledgements

The German ACSYS project was funded by the BMBF, the Artist Project by an EU grant no. ENV4-CT97-0487. Christian Haas contributed to the tools for evaluation of the laser data. We are very grateful to two anonymous reviewers, whose helpful comments have contributed to an improvement of the manuscript.

REFERENCES

Arya, S. P. S. 1973. Contribution of form drag on pressure ridges to the air stress on Arctic ice. *J. Geophys. Res.* **78**, 7092–7099.

Arya, S. P. S. 1975. Drag-partioning theory for determining the large-scale roughness parameter and wind stress on Arctic pack ice. *J. Geophys. Res.* **80**, 3447–3454.

Arya, S. P. S. and Shipman, M. S. 1981. An experimental investigation of flow and diffusion in the disturbed boundary layer over a ridge, 1. Mean flow and turbulence structure. *Atmos. Environ.* **15**, 1173–1184.

Augstein, E. and Cruise Participants 1997. The Expedition Arctic'96 of RV Polarstern (ARK XII) with the Arctic Climate System Study (ACSYS). *Reports on Polar Research* **234**, Alfred Wegener Institute, Bremerhaven, Germany, 54 pp.

Banke, E. G. and Smith, S. D. 1975. Measurement of form drag on ice ridges. *AIDJEX Bull.* **28**, 21–27.

Dierking, W. 1995. Laser profiling of the ice surface topography during the Winter Weddell Gyre Study 1992. *J. Geophys. Res.* **100**, 4807–4820.

Garbrecht, T., Lüpkes, C., Augstein, E. and Wamser, C. 1999. The influence of a sea ice ridge on the low level air flow. *J. Geophys. Res. (D20)* **104**, 24,499–24,507.

Guest, P. S. and Davidson, K. L. 1991. The aerodynamic roughness of different types of sea ice. *J. Geophys. Res. (C3)* **96**, 4709–4721.

Haas, C., Liu, Q. and Martin, T. 1999. Retrieval of Antarctic sea-ice pressure ridge frequencies from ERS SAR imagery by means of in situ laser profiling and usage of a neural network In: *Int. J. Remote Sensing* **20**, 3111–3123.

Hanssen-Bauer, I. and Gjessing, Y. T. 1988. Observations and model calculations of aerodynamic drag on sea ice in the Fram Strait. *Tellus* **40**, 151–161.

Hartmann, J., Albers, F., Argentini, S., Bochert, A., Bonafè, U., Cohrs, W., Conidi, A., Freese, D., Georgiadis, T., Ippoliti, A., Kaleschke, L., Lüpkes, C., Maixner, U., Mastrantonio, G., Ravegnani, F., Reuter, A., Trivellone, G. and Viola, A. 1999. Arctic radiation and turbulence interaction study. *Reports on Polar Research* **305**, Alfred Wegener Institute, Bremerhaven, Germany, 81 pp.

Hartmann, J., Kottmeier, C., Wamser, C. and Augstein, E. 1994. Aircraft measured atmospheric momentum, heat and radiation fluxes over Arctic sea ice. *The polar oceans and their role in shaping the global environment, Geophys. Monogr. Ser.* **85**, ed. by O. M. Johannessen et al., AGU, Washington, D.C., USA, 443–454.

Heygster, G. and Kaleschke, L. 2000. Sea ice remote sensing. In: Final report on the Arctic Radiation and Turbulence Interaction Study (ARTIST), Contract Nr. ENV4-CT97-0497-0487 (DG12-ESCY), Alfred Wegener Institute, Bremerhaven, Germany, 92–105.

Hibler, W. D., Weeks, W. F. and Mock, S. J. 1972. Statistical aspects of sea-ice ridge distributions. *J. Geophys. Res.* **77**, 5954–5970.

Joffre, S. M. 1983. Determining the form drag contribution to the total stress of the atmospheric flow over ridged sea ice. *J. Geophys. Res.* **88**, 4524–4530.

Kottmeier, Ch., Hartmann, J., Wamser, C., Bochert, A., Lüpkes, C., Freese, D. and Cohrs, W. 1994. Radiation and Eddy Flux Experiment 1993 (REFLEX II), *Reports on Polar Research* **133**, Alfred Wegener Institute Bremerhaven, Germany, 62 pp.

Lensu, M., Haas, C., Cottier, F., Friedrich, C., Weisenberger, J., Abrahamsson, K., Ekdahl, A., Darovskikh, A. and Johnsen, K. P. 1996. Arctic '96: Polarstern Ice Station Report. *M-series report* **M 214**, Helsinki University of Technology, Helsinki, Finland, 91 pp.

Lüpkes, C. and Schlünzen, K. H. 1996. Modelling the convective boundary-layer with different turbulence parameterizations. *Boundary-Layer Meteorol.* **79**, 107–130.

Mai, S., Wamser, C. and Kottmaier, C. 1996. Geometric and aerodynamic roughness of sea ice. *Boundary-Layer Meteorol.* **77**, 233–248.

Mellor, G. L. and Yamada, T. 1974. A hierarchy of turbulence closure models for planetary boundary layers. *J. Atmos. Sci.* **31**, 1791–1806.

Mock, S. J., Hartwell, A. D. and Hibler, W. D. 1972. Spatial aspects of pressure ridge statistics. *J. Geophys. Res.* **77**, 5945–5953.

Schlünzen, K. H. 1990. Numerical studies on the inland penetration of sea breeze fronts at a coastline with tidally flooded mudflats. *Beitr. Phys. Atm.* **63**, 254–256.

Wadhams, P. 1980. A comparison of sonar and laser profiles along corresponding tracks in the Arctic Ocean. In: *Sea ice processes and models* (ed. R. S. Pritchard). Proceedings of the Arctic Ice Dynamics Joint Experiment, University of Washington Press, 283–299.

Wyngaard, J. 1973. On surface-layer-turbulence. In: *Workshop on Micrometeorology* (ed. D. Haugen). American Meteorological Society, Science Press, 101–149.